Advanced Detection of COVID-19 Through X-ray Imaging using CovidFusionNet with Hybrid CNN Fusion and Multi-resolution Analysis

Majdi Khalid
Department of Computer Science and Artificial Intelligence-College of Computers, Umm Al-Qura University, Makkah 21955, Saudi Arabia

***Abstract*—The rapid diagnosis of COVID-19 through imaging is crucial in the current pandemic scenario. This study introduces the CovidFusionNet, a novel model adapted for efficient COVID-19 image classification. By effectively combining fusing features from seven pre-trained convolutional neural networks (CNNs), our model presents better accuracy in detecting COVID-19 from X-ray images. Three separate datasets, obtained from Kaggle, were used in this study to ensure the reliability and robustness of the model. The Continuous and Discrete Wavelet Transform was implemented for robust multi-resolution image analysis to maintain image properties after denoising. A novel enhancement method was also proposed, combining the capabilities of Adaptive Histogram Equalization (AHE) and Wavelet Transforms to emphasize finer details and concurrently heighten clarity while minimizing noise. Furthermore, to mitigate class imbalance, an oversampling approach was implemented. Comprehensive validation using 12 metrics across each dataset verified the proposed consistent performance, with remarkable accuracies of 98.02% for Dataset One, 99.30% for Dataset Two, and 98.25% for Dataset Three. Comparing CovidFusionNet against seven well-known pre-trained models showed that CovidFusionNet appeared more capable. This research advances the area of image-based diagnosis using COVID-19 and provides a model for quick medical actions.**

***Keywords*—COVID-19 diagnosis; X-ray imaging; wavelet transform; Adaptive Histogram Equalization (AHE); oversampling; image denoising; image classification**

I. INTRODUCTION

COVID-19 is a novel infectious disease caused by a new flu virus. It first emerged in Wuhan, China, in December 2019 [1]. It's one of the largest worldwide challenges of the 21st century [2, 3]. In March 2020, the World Health Organization (WHO) stated it was a widespread epidemic [4, 5]. COVID-19 is similar to other diseases like MERS and SARS since they all originate from the coronavirus family and harm our lungs [6, 7]. People with COVID-19 could cough, have a fever, feel tired, and lose their sense of taste and smell [8]. Some feel severely ill, have difficulties breathing, or even face life-threatening conditions, including kidney failure [9]. Many individuals died from it globally [10]. Thankfully, numerous companies have created vaccinations and various testing are being done over the world.

Finding persons with COVID-19 quickly is critically crucial to stop it from spreading. One approach to test for it is called RT-PCR [11, 12]. This test takes roughly four to six hours to display results. But, since so many people require testing, laboratories grow incredibly busy and cannot test everyone quickly enough [13]. This means a few people do not get diagnosed and may transmit the infection to others. We need a speedier, automated mechanism to test individuals. It would be beneficial to develop a simpler test that returns answers even sooner, so everyone can know whether they have the virus.

The rapid spread of the COVID-19 pandemic has necessitated the development of effective diagnostic tools for its timely detection. Chest X-ray imaging has emerged as a pivotal diagnostic method to assess the impact of the virus on the lungs. To enhance the efficiency and accuracy of detecting COVID-19 from X-ray images, researchers have proposed various computational methods, primarily harnessing the potential of deep learning. These models aim to swiftly identify patterns indicative of the virus, thereby aiding quicker clinical interventions. This literature review delves into multiple approaches undertaken by researchers worldwide, offering a comprehensive understanding of the advancement in this domain.

In research [14], Terry Gao and Grace Wang employed a set of lung X-ray images that were used to train a deep CNN that can distinguish between noise and useful information. This CNN can then use the data to train and interpret new images by spotting patterns that point to COVID-19. Singh et al. in study [15] suggested the Covid-aid model, an extension of the DarkCovidNet's architecture. With 19 convolution layers and six max-pooling layers, the model defines the lung X-ray images to determine normal, COVID-19 and pneumonia. Though the model could successfully classify the data, the classification accuracy is only 87%. Similarly, Shah et al. [16] proposed a hybrid model that employs a convolutional neural network (CNN) and Gated Recurrent Unit (GRU) to classify the diseases. The CNN model performs feature extraction in this study, whereas the GRU serves as an image classifier. The model is trained and validated with 200 epochs, and on the final epoch, the validation accuracy is as high as 93%. In [17], Khan et al. proposed a CNN architecture to classify COVID-19 pneumonia. The model is constructed employing the transform-merge block (STM) and RE-based operation for feature extraction. Among the three datasets used on the study, the proposed model performs best on the CoV-NonCoV-15k dataset with an accuracy rate of 96.53%.

To classify COVID-19 from chest X-ray images, Gayathri et al. in [18] have proposed an ensemble model after experimenting with several pre-trained model. Among the experimented models, the best outcome was observed from the fusion of the InceptionResNetV2 and Xception models with an accuracy of 95.78%. However, the outcome only depends on the conditions under which the Sparse autoencoder is used for dimensionality reduction and a Feed Forward Neural Network is employed for COVID-19 detection. Banerjee et al. [19] proposed a random forest meta-learning blending algorithm. The strategy follows the decision score technique. For feature extraction of the X-ray images, DenseNet201 architecture is implemented. However, the model only performs well when the dataset is small. On the small Chowdhury et al.'s dataset, the model showed an accuracy rate of 98.13%, whereas, on the larger Wang et al.'s COVID-X dataset, the accuracy was 94.55%.

In the paper [20], Ismael et al. has proposed multiple approaches to classify COVID-19 from the chest X-ray images using deep learning-based models. The study used several CNN models to extract features from the image data. With the assistance of ResNet50 deep feature extractor, the SVM classifier obtained a classification accuracy of 94.7%. Additionally, the authors suggested a fine-tuned CNN model that gives an accuracy rate of 92.6% for the same image data. However, in this study, the lowest accuracy of 91.6% was obtained from a CNN model with end-to-end training. It can be understood that deep approaches are more efficient in the classification of COVID-19 X-ray image data. In study [21], Kanjanasurat et al. used a combination of CNN and RNN techniques. In this study, the fully connected layers of the CNN model, ResNet152V2, were replaced by the RNN model, GRU, to achieve a classification accuracy of 93.37%. Here, the CNN layers were responsible for extracting the features of the data and calculation of dependencies and classification were performed by the RNN layers.

For the classification of chest X-ray images obtained from various sources, Alshmrani et al. suggested a VGG19 model with a fully connected network [22]. The model is assisted by CNN model for feature extraction. This technique provides an accuracy of 96.48% for image classification. In study [23] using ensemble method, Kuzinkovas et al. suggested a model where ANN, LR, LDA and RF performs the task of image classification with an accuracy of 98.34%. During the classification task, the ensemble model uses ResNet50, VGG19, VGG16, and GLCM for feature extraction. Another CNN-based model was suggested by Hafeez et al. in [24] for COVID-19 classification. The proposed CODSC-CNN is consisted of 8 weighted and two fully connected layers. The model is inspired by the pre-trained AlexNet and VGG16 models. The model has an 89% success rate in identifying COVID-19 X-ray images.

Based upon prior research (see Table I) in the area of COVID-19 image identification, we found a few drawbacks in the present approaches. Particularly, several of these models struggle with challenges relating to accuracy, the complexity of managing unbalanced image datasets, and the limitation of constrained data availability. In an attempt to solve these inadequacies and improve the diagnostic effectiveness, we developed the CovidFusionNet. Our proposed model combines the capabilities of multiple pre-trained models to offer higher performance and attain exact identification of COVID-19 in imaging data. By employing an ensemble method, CovidFusionNet seeks to create a new standard in terms of accuracy and durability in COVID-19 identification via imaging. The primary motivation of CovidFusionNet is to optimize the efficiency and precision of COVID-19 diagnosis by exploiting medical imaging, particularly X-ray images. This involves providing medical professionals with a dependable and effective method to detect COVID-19 cases. This is essential due to the fast virus transmission and the need for immediate action. The main contributions in this paper are as follows:

- Proposed a novel fusion model, CovidFusionNet that effectively utilizes the features of multiple pre-trained CNNs to improve COVID-19 image classification. This strategic fusion model assures CovidFusionNet heightened accuracy and flexibility in identifying COVID-19 cases.
- Introduced the use of the Continuous and Discrete Wavelet Transform for multi-resolution analysis. This transformation retains the image's pixel value distributions, ensuring features are preserved during denoising.
- Proposed a novel enhancement method that combines the strengths of AHE and Wavelet Transforms. The method focuses on intricate details, simultaneously enhancing and minimizing noise for optimal image clarity.
- Recognized the presence of class imbalances in the datasets and applied an over-sampling approach, ensuring unbiased model performance.
- We employed 12 evaluation metrics across three distinct datasets to assess the model's reliability and consistency. This thorough evaluation confirms our model's ability to consistently perform well across various datasets, underscoring its adaptability and reliability. Furthermore, we compared the performance of our proposed model with seven pre-trained models to demonstrate its superior capabilities and enhancements.

The structure of the remainder of the paper is organized as follows: Section II presents the data collection process, data preprocessing techniques, handling, and the overall methodology of the proposed framework. Section III delves into the findings and results obtained from applying the proposed method. Section IV provides a comprehensive discussion on these findings, exploring their implications and significance. Section V provides the paper's final section, summarizing the main results and presenting valuable perspectives on possible future research areas in this field.

II. PROPOSED METHOD

In this study, we utilized a systematic strategy to diagnose COVID-19 through imaging. Using three distinctive Kaggle-sourced X-ray datasets, our initial step was image denoising using Continuous and Discrete Wavelet Transforms.

Additionally, a unique improvement approach, merging Adaptive Histogram Equalization (AHE) and Wavelet Transforms, was applied for the enhancement of the image. Recognizing the difficulty of data imbalance, an oversampling approach was applied. The main component of our technique, the CovidFusionNet, fuses feature from seven pre-trained CNNs, achieving greater accuracy. Rigorous validation was undertaken across measures, and comparison analyses were made against renowned pre-trained models. The entire procedure is portrayed in Fig. 1.

TABLE I. A CONCISE OVERVIEW OF CONTEMPORARY DEEP LEARNING RESEARCH ON X-RAYS OF COVID-19

Reference	Dataset	Methodology	Limitations
2020 [14]	Middlemore Hospital data Kaggle	CNN	Small dataset, training set is unknown, lack of details performance metrics
2021 [15]	Joseph Paul Cohen's GitHub repository ChestX-ray8 database structured by Wang et al.	Covid-Aid	Limited and imbalanced dataset, accuracy can be improved.
2021 [16]	Joseph Paul Cohen's GitHub repository Kaggle repository	CNN +GRU	Small and limited dataset, limit to perform on multiple data.
2021 [17]	CoV-Healthy-6k CoV-NonCoV-10k CoV-NonCoV-15k	STM-RENet	Inadequate data preparation and variability in image interpretation.
2022 [18]	Joseph Paul Cohen's GitHub repository Paul Mooney's Kaggle repository	InceptionResNetV2 + Xception	Limited dataset and absence of comparative analysis of pre-trained methods.
2022 [19]	Wang et al.'s dataset (COVID-X) Chowdhury et al.'s dataset	Blended Ensemble	Accuracy can be enhanced, insufficient preprocessing, and lack of model assessment.
2021 [20]	Github, 2020 Kaggle, 2020 Radiology Assistant 2020	Finetuned ResNet50, CNN, ResNet50 + SVM	Model performance can be enhanced, and imbalance dataset.
2023 [21]	Joseph Paul Cohen's GitHub repository Chowdhury et al.'s dataset Kang's dataset Kermany's dataset	ResNet152V2 + GRU	Imbalance dataset, lack of existing model evaluation, and comparatively low accuracy rate.
2023 [22]	Various Public datasets RSNA + SIRM + Radiopaedia Various research articles	VGG19 + CNN	Inadequate model evaluation
2023 [23]	COVID-QU-Ex dataset	ANN+ LR+ LDA+RF	The absence of diverse datasets for model assessments
2023 [24]	COVID19 dataset (2020) Kaggle repository	CNN	Decreased accuracy with varied datasets

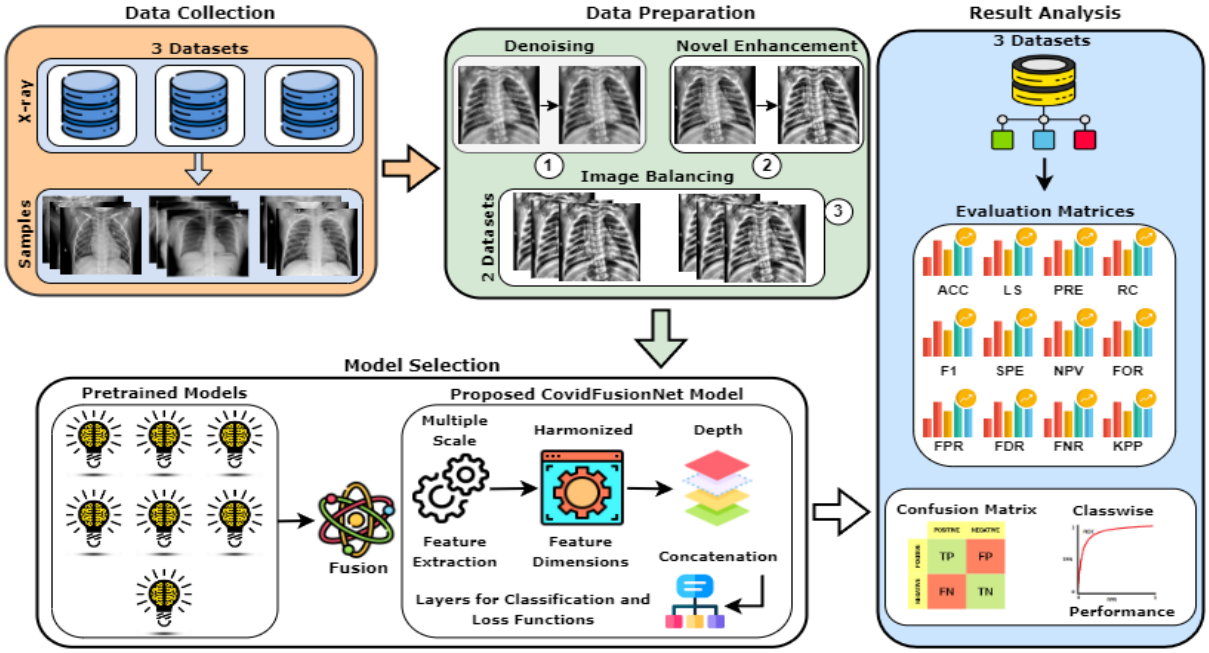

Fig. 1. Proposed workflow of our study for COVID-19 detection.

A. Data Dimensions

For the study on COVID-19 identification, we acquired three different datasets from Kaggle. The first dataset comprises 4,551 X-ray images. Among them, 1,281 images are COVID-19, whereas the remaining 3,270 are normal. This dataset is a compilation of COVID-19 Chest X-ray images gathered by aggregating 15 publicly accessible datasets. The second dataset gives us 4,626 images, split equally, with 2,313 indicating COVID-19 abnormalities and the other 2,313 being normal. The X-ray data used in this second dataset were obtained from numerous sources, such as the GitHub repository, Radiopaedia, the Italian Society of Radiology (SIRM), and the Figshare data repository sites. Our third and final dataset contains 2,159 X-ray images, out of which 576 show COVID-19 features, while 1,583 are categorized as normal. Fig. 2 displays the samples of three datasets. To improve our study's accuracy, we implemented several preprocessing methods. These comprised Image Denoising, Image Enhancement, and Image Balancing. These processes helped make the images more apparent, ensure they were accurately recognized, and make the data more consistent.

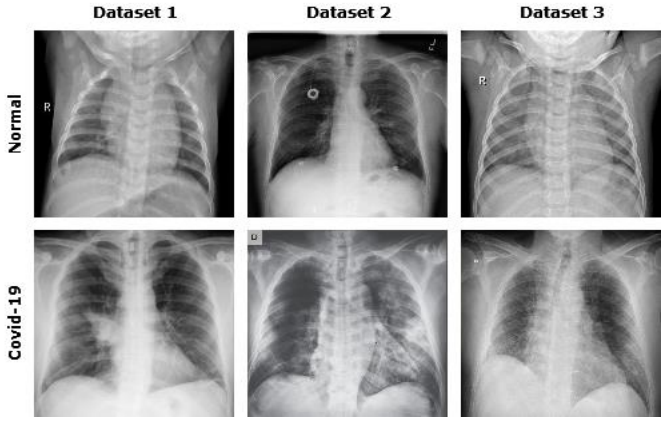

Fig. 2. Sample images from all three datasets.

B. Data Preparation

Data preparation is crucial since it eliminates inconsistencies and inaccuracies, assuring data accuracy. It prepares data for study by reducing noise and irrelevant information [25]. Preprocessing assists in discovering patterns that could be hidden in raw data. Ultimately, it boosts the performance and reliability of deep learning models.

1) Wavelet Transformation (Image Denoising): The Wavelet Transform enables a multi-resolution analysis of a given function or signal by describing it in terms of basic functions obtained from the dilation and translation of a prototype function, nicknamed the "mother wavelet," indicated a $\Psi(t)$. For the Continuous Wavelet Transform (CWT), the transform of a function $f(t)$ can be described as:

$$\boldsymbol{W_f(a,b) = \frac{1}{\sqrt{|a|}} \int_{-\infty}^{\infty} f(t)\Psi(\frac{t-b}{a})dt} \quad (1)$$

Here, $W_f(a, b)$ denotes the wavelet coefficient, with a being the dilation parameter and b the translation parameter. The transformation process encompasses the complete domain of f(t). Crucially, the selected mother wavelet Ψ(t) must conform to the admissibility requirement, defined as:

$$\boldsymbol{C_\Psi = \int_{-\infty}^{\infty} (\frac{|\Psi\hat{}(f)|^2}{|f|}) df < \infty} \quad (2)$$

In this instance, $\Psi\hat{}(f)$ stands for the Fourier transform of $\Psi(t)$. When transferring to the domain of discrete signals, especially crucial for digital applications, the Discrete Wavelet Transform (DWT) becomes increasingly significant. In the DWT, the continuous parameters a and b are discretized, generally specified as $a = 2^m$ and $b = n2^m$, with m and n being integers. This discretization allows a hierarchical examination of the function. The DWT is applied in both row and column directions for two-dimensional data such as images. This leads to four sets of coefficients capturing different information: the approximation (LL), horizontal (LH), vertical (HL), and diagonal details (HH). A fundamental virtue of the wavelet transform is its reversibility, allowing for the original function or image to be rebuilt from its wavelet coefficients using the inverse wavelet transform. Fig. 3 illustrates the output of the Wavelet Transformation with its histogram. The histograms of the original and reconstructed images are remarkably similar, it shows that the wavelet transform (and its inverse) has successfully retained the pixel value distributions of the original image. This positive indicator shows that the wavelet transformation has kept the image's features well.

Algorithm 1. Hybrid AHE-Wavelet Image Enhancement (HAWIE)

```
Procedure HAWIE (Image I, SavePath S)
    Load necessary libraries: numpy, OpenCv, PyWavelets, Matplotlib
    function AHE_Enhancement (Image)
        Apply Adaptive Histogram Equalization on the Image
        return Enhanced image using AHE
    end function
    function Wavelet_Enhancement (Image)
        Convert image to floating-point representation
        Decompose image into wavelet coefficients
        Modify wavelet coefficients
        Reconstruct image from modified coefficients
        return wavelet-enhanced image
    end function
    I_AHE = AHE_Enhancement (Image I)
    I_Enhanced = Wavelet_Enhancement (I_AHE)
    if SavePath S is provided then
        Save I_Enhanced to S
    end if
    return I, I_Enhanced
end procedure
```

2) Hybrid AHE-Wavelet Image Enhancement (HAWIE): In this study, we proposed a Hybrid AHE-Wavelet image enhancement (HAWIE) method as a novel approach for image improvement. This approach combines the comprehensive contrast refinement of Adaptive Histogram Equalization (AHE) with the multi-resolution capabilities of Wavelet

Transforms. Specifically, AHE concentrates on very small overlapping regions of an image, ensuring that every microscopic feature is properly accentuated, whether in a bright or dark location. Following the AHE process, the Wavelet Transform takes center stage, breaking the image into an array of frequency components. This enables a more focused enhancement, where certain visual elements may be enhanced while any undesired noise is concurrently minimized. Our findings, as illustrated in Fig. 4, give an impressive visual illustration of this hybrid method. The difference image, in particular, emerges as a useful tool, clearly emphasizing places that have received adjustments or upgrades. This visualization becomes even more informative when matched with the accompanying scatter plot, where the X-axis indicates pixel values from the original image. At the same time, the Y-axis exhibits those from the improved image. Each point on this figure encapsulates a pixel, its position demonstrating the association between the original and enhanced pixel values. The deviations from the "Line of Identity", a red dashed line showing identical pixel values in both images, give essential insights into the transformational power of the HAWIE approach, emphasizing its capabilities, particularly in vital sectors such as medical imaging. Algorithm 1 provides the overview structure of HAWIE.

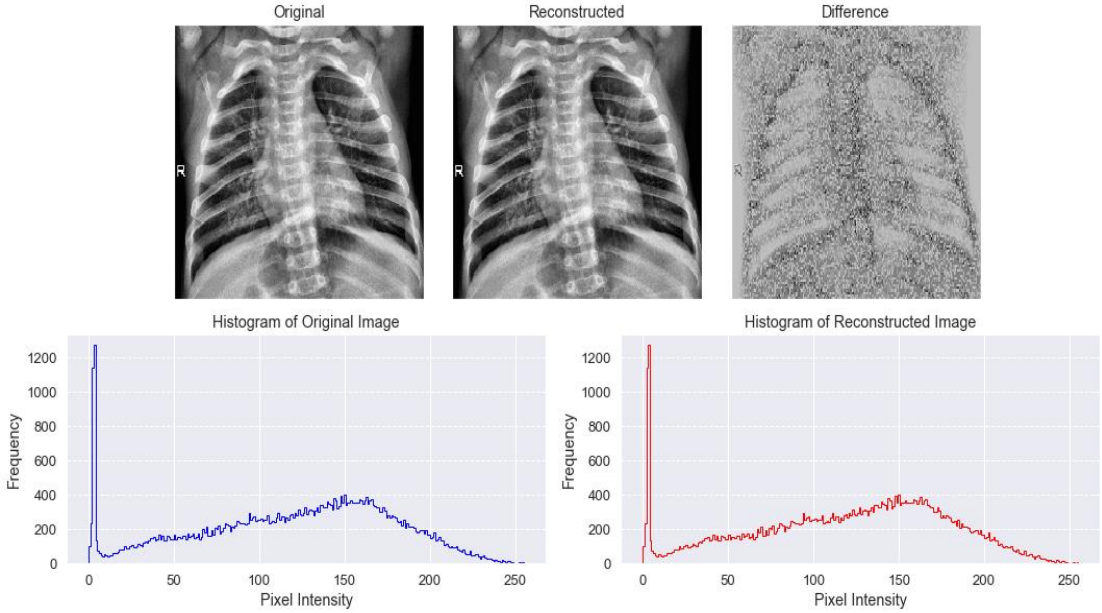

Fig. 3. Output of the wavelet transform with the histograms of the original and reconstructed images. The histogram comparison highlights the wavelet transform's efficacy in maintaining the image's features.

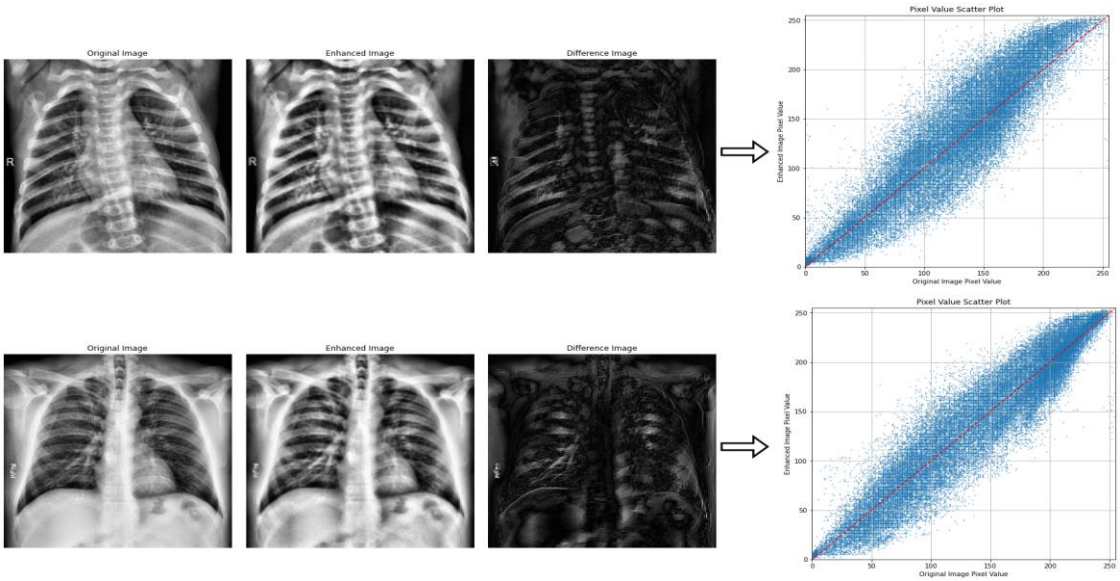

Fig. 4. Illustration of the HAWIE technique effects. The difference image reveals regions of enhancement, while the scatter plot showcases the relationship between original and enhanced pixel values, with deviations indicating modifications.

3) Image Balancing (Oversampling): In this study, we utilized three datasets for analysis. While Dataset 2 was already balanced, Datasets 1 and 3 demonstrated class imbalance, where some classes contained fewer samples than others. This mismatch may lead to biased model performance, perhaps favoring the more dominant classes. We utilized an oversampling approach to solve this difficulty, particularly for the minority classes in Datasets 1 and 3.

The oversampling approach operates by first selecting the class with the maximum number of samples, known as max_count. This count then sets the aim for all classes in the balanced dataset. For those classes with samples less than max_count, the oversampling strategy duplicates their samples until this goal number is attained. Replication is cyclic, meaning that once the end of a class's sample list is reached, it returns to the beginning, assuring a smooth continuation until the target sample count is attained. By applying this strategy, every class in the enlarged datasets (Datasets 1 and 3) now has an equal representation. This parity creates a balanced basis for subsequent data modeling and analysis. By executing this oversampling programmatically, the balanced datasets were stored in a different directory, guaranteeing clarity for later operations. The ultimate purpose of this technique is to reinforce the models' generalizability, trained on the modified datasets, ensuring they give unbiased insights unaffected by the over-representative classes of the original datasets. Table II represents the final datasets after all preprocessed attempts.

TABLE II. DISTRIBUTION OF SAMPLES ACROSS CLASSES IN DATASETS 1, 2, AND 3, ILLUSTRATING POST-OVERSAMPLING

Parameters	Dataset 1	Dataset 2	Dataset 3
Wavelet Transformation	✓	✓	✓
HAWIE	✓	✓	✓
Oversampling	✓	--	✓
Total Images	6540	4626	3166
Train (70%)	4578	3241	2216
Test (20%)	1308	925	633
Validation (10%)	654	460	317

C. Model Selection

For our study, we methodically selected seven pretrained models, each known for particular abilities in image processing. We included VGG19 for its comprehensive feature extraction from its deep 19-layer architecture. MobileNetV2 was selected for its best balance between computing performance and accuracy, which is appropriate for real-time activities. AlexNet, a pioneering model from the ImageNet competition, offers a basic baseline. Simultaneously, the innovative residual blocks of ResNet50, the multi-scale feature capture of InceptionV3, the fine-grained classifications from DenseNet201, and the efficiency of Xception each bring unique value. Together, this collection provides for complete performance evaluations across diverse architectures. Building on their distinct strengths, we next combined the special features of all seven deep learning models to develop our proposed innovative fusion model: CovidFusionNet.

1) VGG19: VGG19 is a well-known deep-learning architecture for classification of images [26]. It has 19 layers in total, including 16 convolutional layers, three fully connected levels, and five max-pooling layers. The persistent use of tiny 3×3 convolutional filters with a stride of 1, which are effective at extracting detailed information when stacked in succession, is a distinguishing characteristic of VGG19. VGG19 ensures the capture of detailed patterns at different spatial hierarchies by gradually increasing the number of filters from 64 in the initial layers to 512 in the deeper ones. The convolutional layers are separated by max-pooling layers with a 2×2 filter size and a stride of 2, which down-samples the spatial dimensions while retaining essential information. Following the convolutional layers, there are three fully connected layers, each having 4096, 4096, and 1000 neurons. Each convolutional layer has a ReLU activation to include nonlinearity in the model. While the uniform structure minimizes architectural complexity, the depth of VGG19 necessitates large processing resources. Nonetheless, its architecture has significantly impacted the field, emphasizing the promise of deeper networks for improved picture identification.

2) MobileNetV2: MobileNetV2 is a simplified deep-learning architecture designed for mobile devices and computationally constrained applications [27]. Inverted residuals and linear bottlenecks are central to its architecture, where channels are first reduced using a 1×1 convolution, followed by a 3×3 depthwise convolution, and then enlarged again, optimizing computational efficiency without compromising feature extraction capabilities. The model makes use of depthwise separable convolutions to reduce parameter counts by separating spatial and channel-wise calculations. MobileNetV2 slims its design even further by preceding fully connected layers in favor of average pooling leading into a SoftMax layer, giving it the highest level of efficiency and performance in on device deep learning applications.

3) AlexNet: AlexNet, a significant deep learning architecture, was essential in advancing the deep learning domain, particularly in the classification of images [28]. The network is composed of five convolutional layers, which are followed by three fully connected layers. The use of bigger filter sizes in AlexNet's first layers is a distinguishing feature; particularly, the first convolutional layer has 11×11 kernels with a stride of 4. As the network grows, it utilizes smaller and smaller filters, such as 5×5 and 3×3. AlexNet was among the first to use ReLU as activation functions, overcoming the vanishing gradient issue that afflicted networks that used classic sigmoid activations. Another novel idea introduced was the notion of dropout layers, in which a part of a neuron is randomly deactivated during training to prevent overfitting. The network also used data augmentation methods such as image translations and horizontal flips to increase the quantity and variety of the training dataset, which improved model generalization. AlexNet's exceptional performance entrenched

deep neural networks as the dominant technique for picture classification, setting the framework for future architectural improvements in deep learning.

4) ResNet50: ResNet50, a member of the Residual Network group, transformed deep learning architectures by introducing residual connections, which are referred to as "skip connections." These connections enable the output of one layer to skip one or more following layers before being summed with the output of the latter, so minimizing the vanishing gradient issue and allowing the training of even deeper networks [29]. ResNet50 is made up of 50 layers that are organized as a blend of convolutional and identity blocks. Each block generally has three convolutional layers with filter sizes of 1×1, 3×3, and 1×1, which are used to decrease dimensionality, collect spatial data, and then restore dimensionality. Strides vary depending on the location of the layer, with stride-2 convolutions used to minimize spatial dimensions, half the height and length while doubling the number of filters. One of ResNet50's key characteristics is its capacity to retain information from previous layers, allowing it to capture both low-level and high-level features. Throughout the network, batch normalization and ReLU activation are employed to stabilize training and induce non-linearity. ResNet50's novel architecture, designed for high accuracy in image classification tasks, not only aids deeper model training but also establishes a new benchmark in deep learning, driving further design advances.

5) InceptionV3: InceptionV3 is a well-known deep learning model for image categorization. Its advanced "modules" execute concurrent convolutional processes with various kernel sizes, such as 1×1, 3×3, and 5×5, inside a single layer [30]. This multi-path technique allows InceptionV3 to record various spatial feature hierarchies at the same time, incorporating both granular and larger viewpoints. The use of factorized convolutions, which split bigger filters into smaller, asymmetric ones like 1×3 and 3×1, is one of InceptionV3's innovations, assuring computational efficiency without losing receptive scope. "Auxiliary classifiers" are deliberately put in the network's intermediate layers to push gradients to inner layers and boost regularization. Batch normalization is used consistently throughout the layers, giving stability to the activations and allowing for smoother training dynamics. Despite its sophisticated design, which combines multi-scale feature extraction with computational prudence, InceptionV3 exemplifies what is possible in terms of balancing accuracy and resource needs in the area of deep image classification.

6) DenseNet201: DenseNet201 distinguishes itself among deep learning architectures developed for image categorization by virtue of its remarkable dense connectivity [31]. Unlike the traditional technique, in which each layer gets information only from its immediate predecessor, DenseNet201 guarantees that each layer receives input from all previous levels, resulting in an extensive network of connections. This configuration encourages feature reuse and ensures more efficient gradient flow across the network, solving issues such as the disappearing gradient problem, which is common in deep architectures. Each layer, which is divided into interconnected blocks, generally employs 3×3 convolutional filters, with precise growth rates defining the insertion of additional filters as the network deepens. To regulate and aggregate feature-map dimensions, transition layers of 1×1 convolutional filters with a stride of 2 are alternated between these dense blocks. DenseNet201, with its 201 layers, is capable of collecting sophisticated image patterns without a massive rise in parameters due to its dense design. DenseNet201's architecture, which emphasizes continuous feature propagation and efficient gradient distribution, makes it highly resistant to overfitting and places it as a model of choice for complex image classification tasks.

7) Xception: Xception, which stands for "Extreme Inception," is a complex classification architecture that redefines the traditional inception technique by using depthwise separable convolutions [32]. This fundamental breakthrough divides convolutional processes into spatial and channel-based tasks, maximizing efficiency. The Xception model is composed of 71 layers that are organized into modules. Unlike standard Inception modules, which utilize a variety of filter sizes, Xception's architecture relies heavily on 3x3 convolutional kernels for depthwise operations, ensuring a thorough extraction of spatial data. 1x1 convolutions are utilized for cross-channel operations inside these modules. The model achieves strategic downsampling by adopting strides of 2 in selected modules. Xception incorporates residual connections, similar to the ResNet structure, to maintain smooth gradient flow throughout its depth, further strengthening its resilience. Xception proposes an architecture that delivers outstanding performance on picture classification tasks while assuring computational economy by combining the ideas of depthwise separable convolutions, intentional kernel choices, and a thoughtfully built layering scheme.

8) CovidFusionNet (Proposed Model): In this study, we proposed a novel CovidFusionNet model to increase classification performance, particularly for differentiating images related to COVID, by combining the strength of numerous pre-trained convolutional neural networks (CNNs) and their feature extraction capabilities.

The CovidFusionNet model begins by representing each image as I with a shape of 224×224×3. For each base model m within our ensemble model M (which encompasses seven models), the image undergoes a transformation through function f_m, generating a feature map F_m according to the equation 3:

$$F_m = f_m(I) \tag{3}$$

A harmonizing step is essential due to the varied spatial dimensions of the feature maps yielded by the different architectures. A resizing function, represented as R, refines each feature map to achieve a uniform shape:

$$F'_m = R(F_m) \tag{4}$$

Resultantly, F'_m is consistent with a dimension of 224×224×d_m, where d_m marks the depth as per model m. The essence of CovidFusionNet lies in its strategic feature fusion. Feature maps from all models are concatenated in depth, forming an integrated tensor F_c:

$$F_c = Concatenate\ (F'_{vgg16}, F'_{mobilenetv2}, \ldots\ldots, F'_{xception}) \quad (5)$$

After this fusion, F_c undergoes flattening and is channeled through a series of dense layers. Initially, it interacts with a weight matrix W_1 and bias b_1 to produce an output:

$$o_1 = ReLU\ (v.W_1 + b_1) \quad (6)$$

Post the application dropout regularization for model robustness, the final output is calculated as:

$$O = Softmax\ (o_1.W_2 + b_2) \quad (7)$$

The Categorical Cross entropy loss L supervises the training of the CovidFusionNet:

$$L = -\sum_{i=1}^{2} Y_i\ log\ (O_i) \quad (8)$$

This ensures optimal weight adjustments during training, directing the model toward accurate COVID-19 detection. Algorithm 2 depicts the operation of the proposed model.

Algorithm 2. Proposed CovidFusionNet Development and Operation

Procedure CovidFusionNet(Image *I*)
    Load pre-trained models into set *M*
    Freeze the weights of the models in *M*
    for each model m in *M* **do**
        Transform image *I* using m to get feature map F_m
        if F_m does not have dimension 7×7×d_m
            Resize F_m to F'_m of dimension 7×7×d_m
        else
            $F'_m = F_m$
        end if
        Store F'_m in list of feature maps *F'*
    end for
    Concatenate feature maps in *F'* along depth to get F_c
    Flatten F_c to get 1D tensor *T*
    O_1 = Dense layer with ReLU activation on *T*
    Apply dropout on o_1
    O = Dense layer with Softmax activation on result
    return O
end procedure

The CovidFusionNet model exhibits remarkable improvements over to prior methodologies in medical image classification, specifically for identifying COVID-19. The main benefit of this approach is the use of numerous pre-trained convolutional neural networks (CNNs), which allows for a more extensive and diverse extraction of features compared to models that rely on a single CNN architecture. The variety of methods used to extract features leads to a classification that is less vulnerable to errors and more precise, which is essential for the specific needs of medical imaging. CovidFusionNet specifically tackles the issue of spatial dimension variability, which is a common occurrence when merging information from various CNNs. The resizing function is utilized to normalize feature maps prior to fusion, promising a consistent and harmonic integration of features. This strategy addresses the constraints associated with the restricted feature representation commonly observed in single-model approaches.

III. Performance Evaluation

Several evaluation metrics were examined to evaluate the efficacy of various deep-learning models. These measures, particularly Accuracy, Loss, Precision, Recall, F1-Score, Specificity, NPV, FOR, FPR, FDR, FNR, and Kappa Score, highlight the efficiency and dependability of the models under assessment. Fig. 5 to Fig. 10 presents a visual illustration of these scores. These figures show an in-depth visual representation of performance metrics [33] for the deep learning models analyzed in our study, including proposed CovidFusionNet (CvNet), VGG19 (VGG), MobileNetV2 (MV2), AlexNet (AxNT), RestNet50 (RsNT), Incep-tionV3 (InV3), DenseNet201 (DSNT), and Xception (XPTN). The metrics are placed across two separate rows inside the image, covering a wide variety of assessment criteria.

A. Performance Evaluation

To evaluate the efficacy of our employed classifiers in identifying COVID-19 from X-ray images, we applied a complete set of evaluation metrics (9) to (20). Where TP, FP, TN, and FN stand for the number of true positive, false positive, true negative and false negative cases, respectively.

Accuracy: Proportion of all X-ray images correctly identified, be it COVID-19 positive or negative.

$$Accuracy = \frac{(TP+TN)}{(TP+FP+TN+FN)} \quad (9)$$

Loss: Quantifies how well the prediction model performs compared to the actual outcomes.

$$Loss = -(y\ log(p) + (1-y)\ log(1-p)) \quad (10)$$

Precision: The percentage of X-rays that were accurately diagnosed as COVID-19 positive.

$$Precision = \frac{TP}{(TP+FP)} \quad (11)$$

Recall: The proportion of true COVID-19 positive X-rays that the model identified.

$$Recall = \frac{TP}{(TP+FN)} \quad (12)$$

F1-Score: Harmonic mean of precision and recall, ensuring a balance between them.

$$F1_{score} = 2 \times \frac{Precision*Recall}{Precision+Recall} \quad (13)$$

Specificity: The percentage of COVID-19 negative X-rays that the model accurately detected out of all the actual images.

$$Specificity = \frac{TN}{(TN+FP)} \quad (14)$$

NPV (Negative Predictive Value): The percentage of X-rays that were appropriately diagnosed as COVID-19 negative.

$$NPV = \frac{TN}{(TN+FN)} \quad (15)$$

FOR (False Omission Rate): percentage of COVID-19 positive cases that were actual but were misclassified as negative by the model.

$$FOR = \frac{FN}{(FN+TN)} \quad (16)$$

FPR (False Positive Rate): The proportion of real COVID-19 negative cases that were misclassified as positive by the model.

$$FPR = \frac{FP}{(FP+TN)} \quad (17)$$

FDR (False Discovery Rate): The proportion of X-rays mistakenly classified as COVID-19 positive but truly negative.

$$FDR = \frac{FP}{(FP+TP)} \quad (18)$$

FNR (False Negative Rate): The percentage of real COVID-19 positive cases that the model failed to predict.

$$FNR = \frac{FN}{(FN+TP)} \quad (19)$$

Kappa Score: Measures validity of predicted and actual classifications, adjusting for chance. A score near to 1 indicates outstanding alignment.

$$K = \frac{P_o - P_e}{1 - P_e} \quad (20)$$

where, p_o is the observed agreement, and p_e is the expected agreement.

B. *Performance for Dataset 1*

From the analysis of dataset 1, CvNet appears as a highly effective classifier, obtaining an ACC of 98.02%. Specifically, with CvNet, we notice an excellent PRE of 98.5%. It is followed at some distance by MV2, which records a score of 91.5%. Moving to the REC criteria, RsNT and InV3 exhibit impressive scores of 86.5%, but CvNet stands out with a significant score of 97.5%. Concerning F1S, whereas XPTN remains with a score of 82.75%, CvNet increases by reaching its highest point with a score of 98%. In terms of Specificity, a parameter important for understanding the real negative rate, CvNet again outperforms with 98.5%, with most other models.

The NPV, FOR, FPR, FDR, FNR, and the Kappa Score further show the capabilities of each model. Notably, CvNet differentiates out across these criteria. With an NPV of 98, it greatly beats VGG, which gets 84.5%. In analyzing the FOR, both VGG and InV3 score on the upper side at 15.5% and 15%, respectively. In comparison, CvNet has a respectable low score of 2%. Focusing on FPR, models like VGG, RsNT, and XPTN indicate heightened values of 15%, 13%, and 17%. Yet again, CvNet excels with a minimum 1.5%. As for FDR, XPTN's rate of 16.5% is in significant contrast to CvNet's low 1.5%. On the FNR front, although XPTN achieves a high 18%, CvNet displays its efficiency with only 2.5%. Lastly, considering the Kappa Score, CvNet's quality shines with 0.96, implying an excellent match with actual labels. On the other hand, XPTN scores 0.66, with MV2 and DSNT coming in between 0.82 and 0.78, respectively. Fig. 5 shows the performance of the models on dataset 1.

Fig. 6 shows the confusion matrix for multiple models, including CvNet, VGG, MV2, AxNT, RsNT, InV3, DSNT, and XPTN, when discriminating between COVID-19 and normal situations. For instance, evaluating the CvNet model, it can be determined that out of the COVID-19 instances, 638 were properly categorized as COVID-19 (True Positives) and 16 were wrongly classified as normal (False Negatives). On the other hand, when evaluating the normal cases, 644 were properly recognized as normal (True Negatives), and 10 were misclassified as COVID-19 (False Positives). Similar classification accuracy and error patterns were also found for the other models. For instance, the VGG model accurately recognized 549 COVID-19 samples but misclassified 105 as normal. Simultaneously, 556 normal samples were identified correctly, whereas 98 were misdiagnosed as COVID-19. However, the performance scores indicate that the CvNet model surpassed all other models in the classification performance for dataset 1.

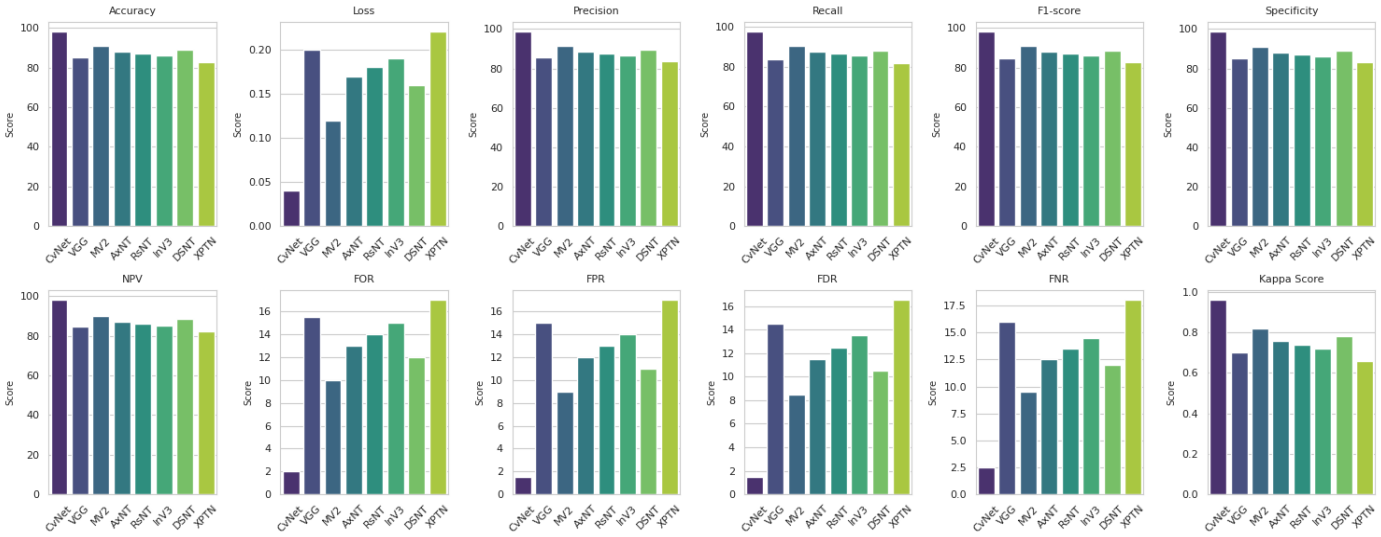

Fig. 5. Comparative performance metrics across the models on dataset 1.

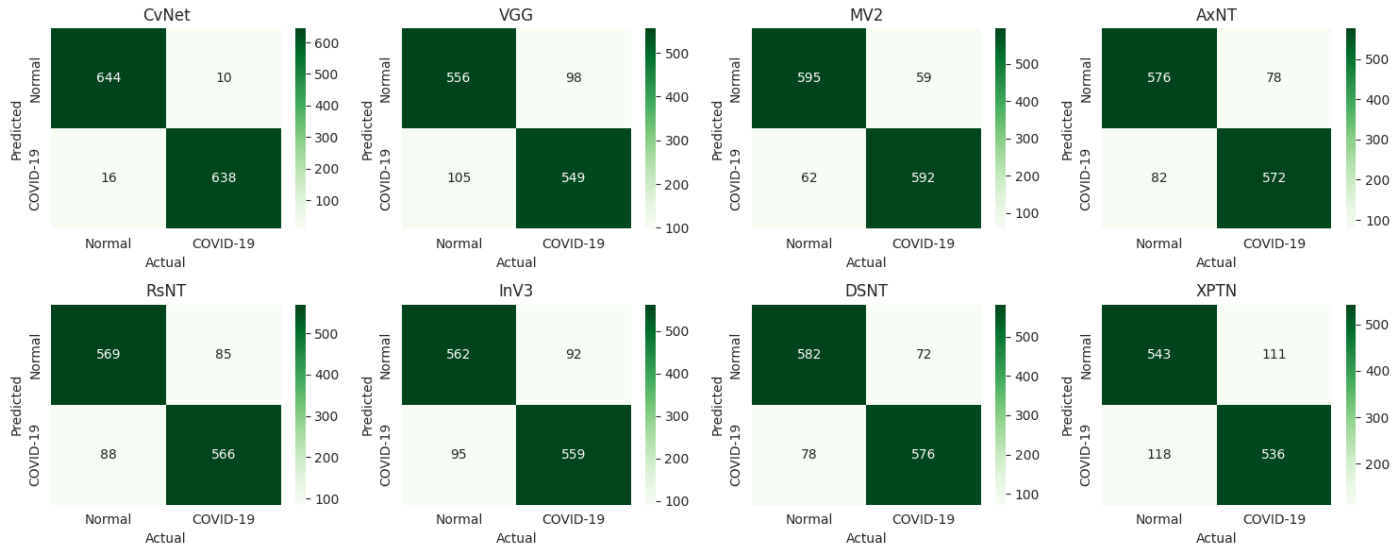

Fig. 6. Confusion matrices of deep learning models for COVID-19 vs. normal classification on dataset 1.

C. Performance for Dataset 2

From the examination of dataset 2, CVNet emerged as the most efficient classifier, obtaining an accuracy of 99.30%. Specifically, with CVNet, we observe an exceptional precision of 99.4%. Following that, MV2 obtained a score of 93.2%. Turning to the recall parameter, RsNT and InV3 exhibit impressive results, but CVNet surpasses with a significant score of 99.2%. In terms of F1-score, whereas Xception (XPTN) achieves a score of 90.10%, CVNet reaches the highest point with a score of 99.30%. For specificity, an essential statistic for distinguishing an actual negative rate, CVNet continues to dominate with 99.3%, outperforming the other models.

Other metrics, including NPV, FOR, FPR, FDR, FNR, and the Kappa Score, further emphasize the capabilities of each model. Furthermore, CvNet differentiates itself across these parameters. With an NPV of 99.3%, it greatly surpasses VGG, which settles at 89.1%. Analyzing the FOR, both VGG and InV3 score better with 10.9% and 16.3%, respectively, although CvNet excels with a low score of 0.7%. Focusing on the FPR, models such as VGG, RsNT, and XPTN exhibit increased rates. Yet again, CvNet outperforms with a minimum 0.7%. In terms of the FDR, XPTN rate of 9.7% compares strongly with CvNet only 0.6%. On the FNR, XPTN displays a higher number, while CvNet demonstrates its efficiency with a modest 0.8%. Finally, while reviewing the Kappa Score, the quality of CvNet shows effectively with 0.986, indicating a nearly perfect agreement with true labels. In comparison, XPTN obtains 0.802, with MV2 and DSNT slowing with their respective scores. Fig. 7 visually represents the model performances with a comprehensive comparison.

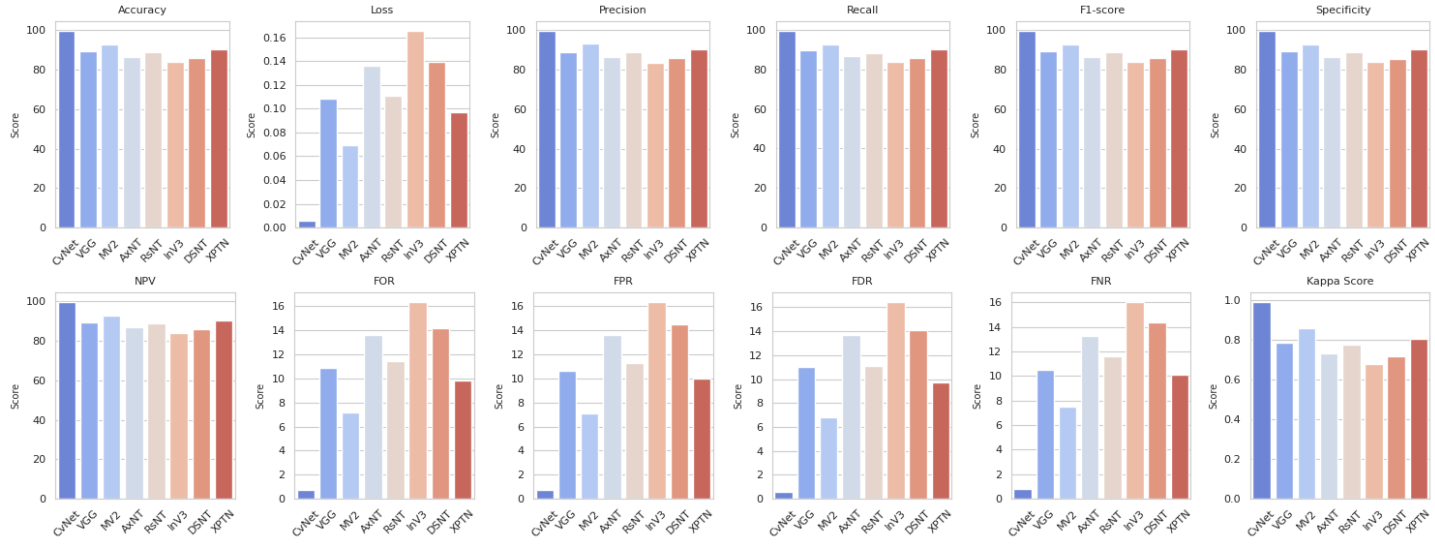

Fig. 7. Comparative performance metrics across the models on dataset 2.

Fig. 8 illustrates the confusion matrix for all of the employed models including CvNet, VGG, MV2, AxNT, RsNT, InV3, DSNT, and XPTN) in the context of identifying between COVID-19 and normal cases. Upon assessing the CvNet model, it's observed that out of the total COVID-19 cases, 495 were accurately recognized as COVID-19 (True Positives), whereas seven were misclassified as normal (False Negatives). In comparison, for the normal cases, 493 occurrences were adequately identified as normal (True Negatives), while five were mislabeled as COVID-19 (False Positives). Observing comparable patterns with different models, take the VGG model as an instance: it correctly recognized 441 occurrences of COVID-19, but mislabeled 61 as normal. Concurrently, out of the normal samples, 439 were appropriately identified, while 59 were incorrectly classed as COVID-19. Despite the variances between models, the performance measures indicate CvNet as the standout, exemplifying higher classification for dataset 2 compared to other models.

D. Performance for Dataset 3

From the assessment of our dataset 3, CvNet emerges as the best classifier with an outstanding accuracy of 98.25%. Specifically, with CvNet, we see an outstanding precision of 98.7%. Besides, MV2 achieves an accuracy of 93.8%. As for the recall, both RsNT and AxNT produced substantial results, CvNet reached out with a higher score of 98%. Moving to the F1-score, though XPTN gains a score of 91.9%, CvNet achieves its highest rating with 98.35%. In specificity, a critical parameter for determining the real negative rate, CvNet maintains its dominance with a remarkable 98.9%, surpassing the other models.

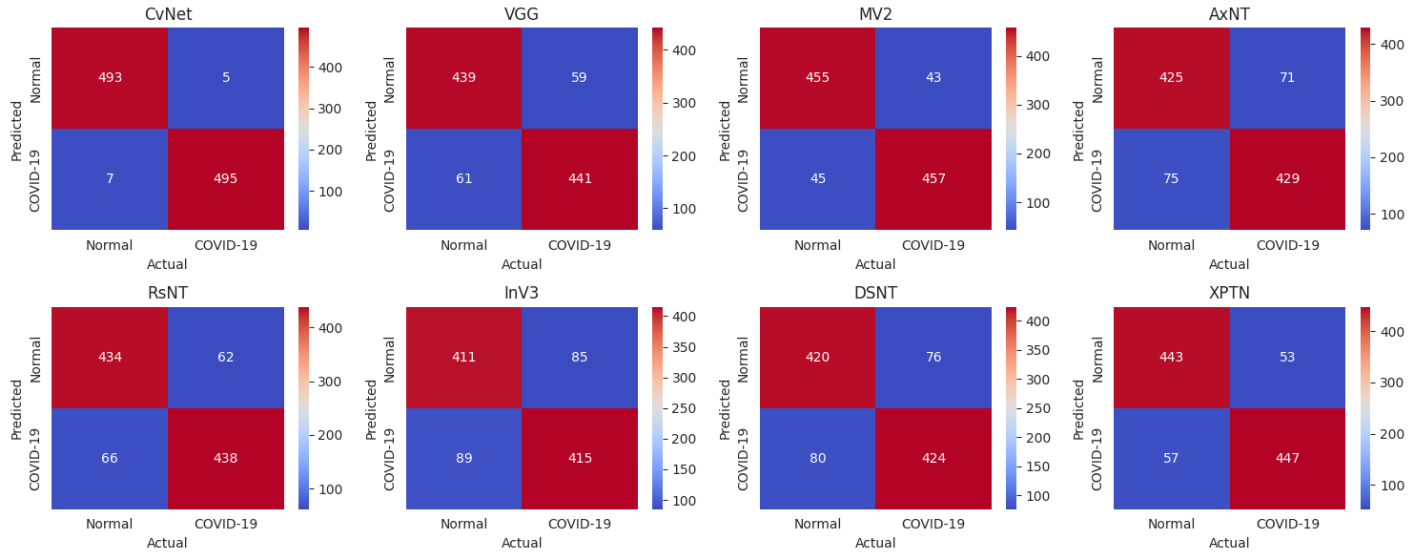

Fig. 8. Confusion matrices of deep learning models for COVID-19 vs. normal classification on dataset 2.

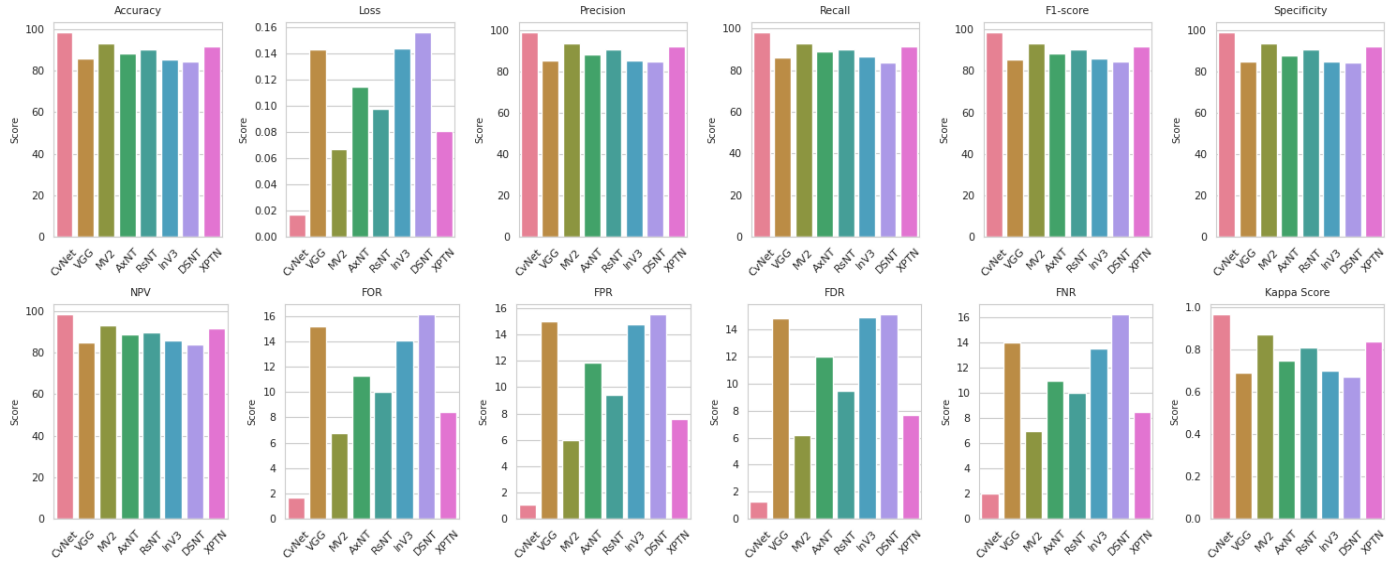

Fig. 9. Comparative performance metrics across the models on dataset 3.

We learn more about each model's effectiveness by exploring other metrics, such as NPV, FOR, FPR, FDR, FNR, and the Kappa Score. CvNet is one of them that sticks out particularly. CvNet significantly exceeds VGG, which has an NPV of 84.8%, with an NPV of 98.3%. In contrast to CvNet's admirable 1.7%, both VGG and DSNT models exhibit greater rates when analyzing FOR, 15.2% and 16.1%, respectively. The VGG, RsNT, and DSNT exhibit greater rates in terms of FPR, CvNet excels with a rate of only 1.1%. In terms of the FDR, XPTN has a respectable rate of 7.7%, whereas CvNet excels with only 1.3%. XPTN has a little higher value while monitoring FNR, however, CvNet performs better with pure 2%. Lastly, CvNet's Kappa Score of 0.965 is remarkable and perfectly matches true labels. This rating distinguishes it from other models like XPTN, MV2, and DSNT. Fig. 9, a visual representation, helps clarify these comparisons and provides an extensive overview of how well the models performed, showing their advantages and possible weaknesses.

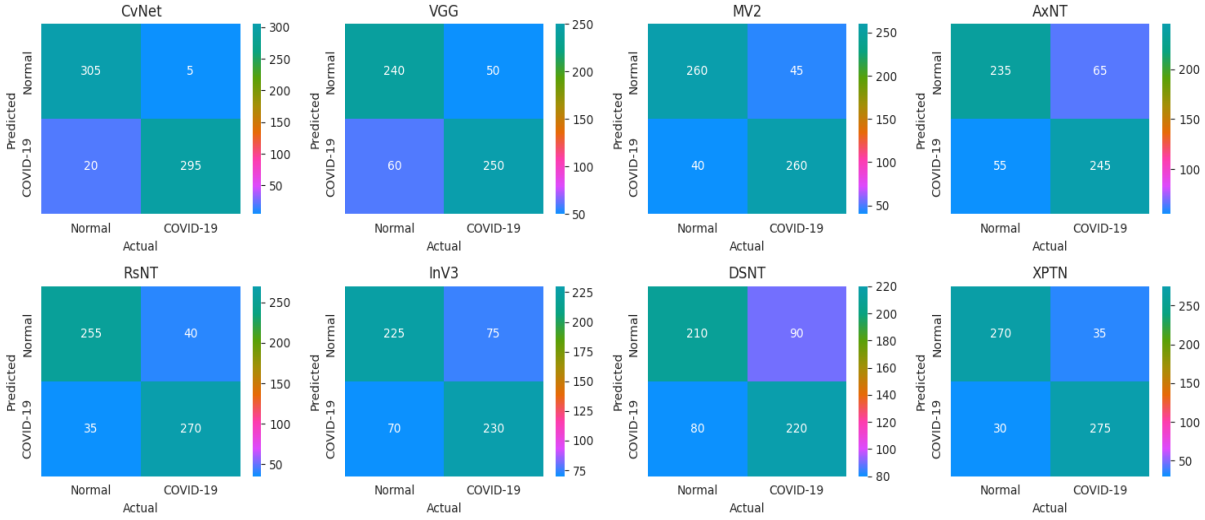

Fig. 10. Confusion matrices of deep learning models for COVID-19 vs. normal classification on dataset 3.

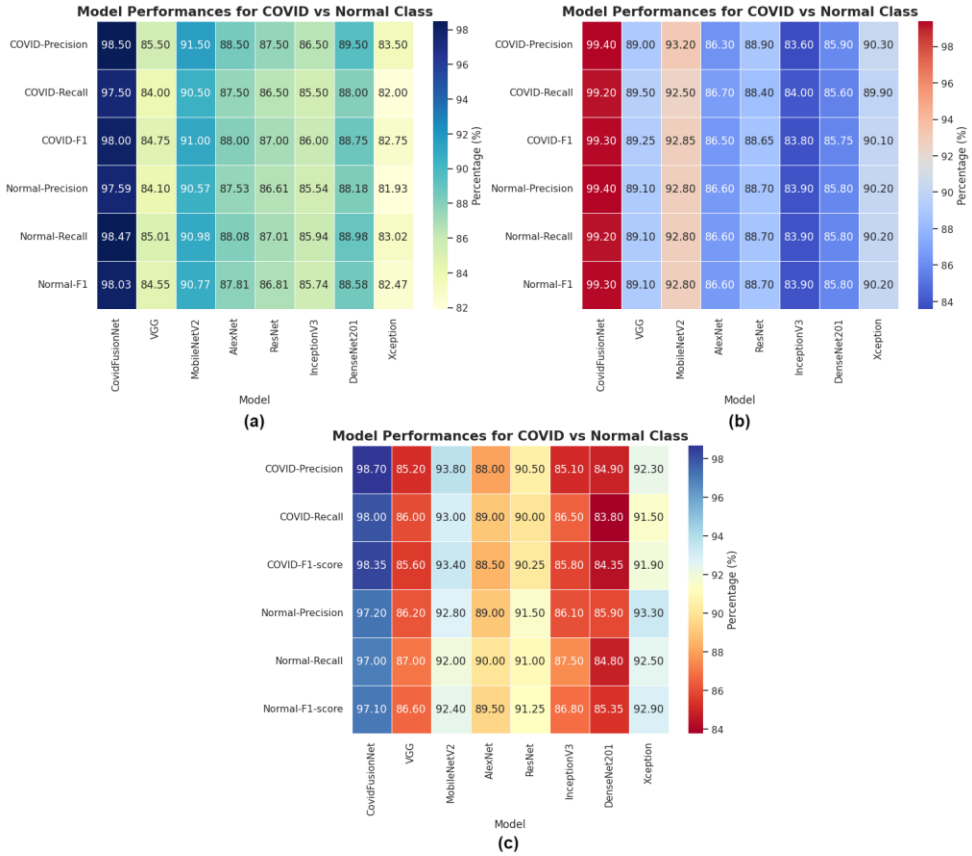

Fig. 11. Class-wise performance metrics of various models for COVID-19 detection across three datasets: (a) Dataset 1, (b) Dataset 2, and (c) Dataset 3

Fig. 10 exhibits the confusion matrices for all the models evaluated, including CvNet, VGG, MV2, AxNT, RsNT, InV3, DSNT, and XPTN, in their attempts to identify COVID-19 and normal cases. A detailed review of the CvNet model indicates that of the total supposed COVID-19 cases, 295 were accurately recognized as COVID-19 (True Positives), whereas 20 were erroneously tagged as normal (False Negatives). Conversely, among the samples identified as normal, 305 were properly marked as normal (True Negatives), with 5 being mistakenly indicated as COVID-19 (False Positives). VGG model properly discovered 250 instances of COVID-19, but wrongly categorized 60 as normal. However, out of the normal samples, 240 were correctly recognized, while 50 were incorrectly categorized as COVID-19. Moreover, CvNet distinguishes itself as being better by classifying Dataset 3 with more accuracy when compared to the other models.

E. Classwise Performance Analysis

Fig. 11(a) exhibiting Dataset 1 indicates that CovidFusionNet produced outstanding accuracy for the COVID class (98.5%). For the COVID class, CovidFusionNet achieved a highest F1-score (98%) whereas ResNet closely followed with an F1-score of 87%. For the Normal class, CovidFusionNet scored the best accuracy value (97.59%) and its recall was equally effective at 98.47%. This implies that for the categories COVID and Normal, while CovidFusionNet outperforms in one measure, other models such as ResNet or AlexNet tend to follow closely, showing their complementing potential. Fig. 11(b) depicting Dataset 2 demonstrates that CovidFusionNet once again came out with the highest accuracy for the COVID class (99.4%). In terms of the COVID class, CovidFusionNet retained the top F1-score (99.30%). For the Normal class, both accuracy and recall values were generally stable across the models, with CovidFusionNet winning once again with an F1-score of 99.3%. The superior performance of CovidFusionNet across these measures reinforces its great competence in discriminating between both classes. Fig. 11(c) from Dataset 3 highlights that CovidFusionNet continues its trend with outstanding accuracy for the COVID class (98.7%). MobileNetV2 obtained an excellent F1-score (93.4%) for the COVID class, whereas for the Normal class, Xception performed amazingly with the top F1-score (92.9%).

IV. DISCUSSION

The CovidFusionNet is specifically designed for high-resolution medical imaging, with a focus on X-ray images. It showcases its capabilities by combining several Convolutional Neural Networks (CNNs) with Wavelet Transforms, which are essential for precise identification of patterns and reliable diagnosis of COVID-19. The oversampling strategy employed by this system enhances its ability to effectively handle datasets with class imbalances, which are often seen in medical data. As a result, this system is especially relevant in the present healthcare scene. In addition, CovidFusionNet's ability to do multi-resolution image analysis, utilizing both Continuous and Discrete Wavelet Transform, enables the detection of anomalies at various scales. Furthermore, integrating Adaptive Histogram Equalization with Wavelet Transforms for image improvement is particularly effective for datasets requiring precise feature retention and noise reduction. Although it demonstrates exceptional performance in these domains, its utilization with other data formats, such as MRI or CT scans, may necessitate appropriate modifications to achieve ideal outcomes. In consideration of this recognition, further study will prioritize the extension of CovidFusionNet's utilization to a range of data formats, thereby thoroughly assessing its efficacy in different clinical environments. This study aims to improve the effectiveness and expand the range of applications of the model in medical imaging, thereby transforming it into a flexible instrument in the advancing field of medical diagnostics. We have compared the performance of our proposed model with state-of-the-art methods, and the comparative results are represented in Table III.

TABLE III. COMPARING PROPOSED METHOD PERFORMANCE WITH STATE-OF-THE-ART METHODS

Reference	Dataset	Methodology	Accuracy
[14]	X-ray	CNN	91%
[15]	X-ray	Covid-Aid	87%
[16]	X-ray	CNN +GRU	93%
[17]	X-ray	STM-RENet	96.53%
[18]	X-ray	InceptionResNetV2 + Xception	95.78%
[20]	X-ray	ResNet50 + SVM	94.7%
[21]	X-ray	ResNet152V2+GRU	93.37%
[22]	X-ray	VGG19 + CNN	96.48%
Proposed	X-ray	CovidFusionNet	Dataset 1 (98.02%)
			Dataset 2 (99.30%)
			Dataset 3 (98.25%)

V. CONCLUSION

In this study, we introduced the CovidFusionNet, a cutting-edge CNN model based on fusion and optimized for accurately classifying COVID-19 X-ray images across three distinct datasets. We improved image clarity and detail preservation by combining features from seven pre-trained convolutional neural networks, incorporating the Continuous and Discrete Wavelet Transform, and using an innovative enhancement technique that combines Adaptive Histogram Equalization and Wavelet Transforms (HAWIE). Our model outperformed seven well-known pre-trained models in accuracy and consistency when combined with an oversampling strategy to solve the class imbalance. This work advances the field of image-based COVID-19 diagnosis by providing a tool ready for clinical use and pointing out potential directions for further investigation into the effects of image quality on detection effectiveness.

Data Availability Statement: Dataset 1 can be found at https://www.kaggle.com/datasets/unaissait/curated-chest-xray-image-dataset-for-covid19 (Accessed on 1 September 2023); Dataset 2 can be found at https://www.kaggle.com/datasets/amanullahasraf/covid19-pneumonia-normal-chest-xray-pa-dataset, (Accessed on 2 September 2023); Dataset 3 can be found at https://www.kaggle.com/datasets/jtiptj/chest-xray-pneumoniacovid19tuberculosis, (Accessed on 2 September 2023).

REFERENCES

[1] R. Huang, M. Liu, and Y. Ding, ‘‘Spatial-temporal distribution of COVID-19 in China and its prediction: A data-driven modeling analysis,’’ J. Infection Developing Countries, vol. 14, no. 3, pp. 246–253, Mar. 2020.

[2] A. C. Cunningham, H. P. Goh, and D. Koh, ‘‘Treatment of COVID-19: Old tricks for new challenges,’’ Crit. Care, vol. 24, no. 1, p. 91, Dec. 2020.

[3] Z. Wang, Y. Xiao, Y. Li, J. Zhang, F. Lu, M. Hou, and X. Liu, ‘‘Automatically discriminating and localizing COVID-19 from community-acquired pneumonia on chest X-rays,’’ Pattern Recognit., vol. 110, Feb. 2021, Art. no. 107613.

[4] D. Cucinotta and M. Vanelli, ‘‘WHO declares COVID-19 a pandemic,’’ Acta Bio Medica, Atenei Parmensis, vol. 91, no. 1, p. 157, 2020.

[5] M. Ndiaye, S. S. Oyewobi, A. M. Abu-Mahfouz, G. P. Hancke, A. M. Kurien, and K. Djouani, ‘‘IoT in the wake of COVID-19: A survey on contributions, challenges and evolution,’’ IEEE Access, vol. 8, pp. 186821–186839, 2020.

[6] H. A. Rothan and S. N. Byrareddy, ‘‘The epidemiology and pathogenesis of coronavirus disease (COVID-19) outbreak,’’ J. Autoimmunity, vol. 109, May 2020, Art. no. 102433.

[7] S. Hu, Y. Gao, Z. Niu, Y. Jiang, L. Li, X. Xiao, M. Wang, E. F. Fang, W. Menpes-Smith, J. Xia, H. Ye, and G. Yang, ‘‘Weakly supervised deep learning for COVID-19 infection detection and classification from CT images,’’ IEEE Access, vol. 8, pp. 118869–118883, 2020.

[8] C. Menni, A. Valdes, M. B. Freydin, S. Ganesh, J. E.-S. Moustafa, A. Visconti, P. Hysi, R. C. Bowyer, M. Mangino, M. Falchi, and J. Wolf, ‘‘Loss of smell and taste in combination with other symptoms is a strong predictor of COVID-19 infection,’’ MedRxiv, 2020.

[9] L. Goyal and N. Arora, ‘‘Deep transfer learning approach for detection of COVID-19 from chest X-ray images,’’ Int. J. Comput. Appl., vol. 975, p. 8887.

[10] M. Awais, M. Raza, N. Singh, K. Bashir, U. Manzoor, S. U. Islam, and J. J. P. C. Rodrigues, ‘‘LSTM based emotion detection using physiological signals: IoT framework for healthcare and distance learning in COVID-19,’’ IEEE Internet Things J., early access, Dec. 10, 2020, doi: 10.1109/JIOT.2020.3044031.

[11] I. Kokkinakis, K. Selby, B. Favrat, B. Genton, and J. Cornuz, ‘‘COVID-19 diagnosis: Clinical recommendations and performance of nasopharyngeal swab-PCR,’’ Revue Medicale Suisse, vol. 16, no. 689, pp. 699–701, 2020.

[12] M. Roberts, D. Driggs, M. Thorpe, J. Gilbey, M. Yeung, S. Ursprung, A. I. Aviles-Rivero, C. Etmann, C. McCague, L. Beer, J. R. Weir-McCall, Z. Teng, E. Gkrania-Klotsas, J. H. F. Rudd, E. Sala, and C.-B. Schönlieb, ‘‘Common pitfalls and recommendations for using machine learning to detect and prognosticate for COVID-19 using chest radiographs and CT scans,’’ Nature Mach. Intell., vol. 3, no. 3, pp. 199–217, Mar. 2021.

[13] C.-C. F. Tam, K. S. Cheung, S. Lam, A. Wong, A. Yung, M. Sze, Y.-M. Lam, C. Chan, T. C. Tsang, M. Tsui, and H. F. Tse, ‘‘Impact of coronavirus disease 2019 (COVID-19) outbreak on ST-segment–elevation myocardial infarction care in Hong Kong, China,’’ Circulat., Cardiovascular Qual. Outcomes, vol. 13, no. 4, 2020, Art. no. e006631

[14] Gao, T., & Wang, G. (2020). Chest X-ray image analysis and classification for COVID-19 pneumonia detection using Deep CNN. medRxiv, 2020-08.

[15] Singh, S., Sapra, P., Garg, A., & Vishwakarma, D. K. (2021, April). CNN based Covid-aid: Covid 19 Detection using Chest X-ray. In 2021 5th International Conference on Computing Methodologies and Communication (ICCMC) (pp. 1791-1797). IEEE.

[16] Shah, P. M., Ullah, F., Shah, D., Gani, A., Maple, C., Wang, Y., Abrar, M., & Islam, S. U. (2021). Deep GRU-CNN model for COVID-19 detection from chest X-rays data. Ieee Access, 10, 35094-35105.

[17] Khan, S. H., Sohail, A., Khan, A., & Lee, Y. S. (2022). COVID-19 detection in chest X-ray images using a new channel boosted CNN. Diagnostics, 12(2), 267.

[18] Gayathri, J. L., Abraham, B., Sujarani, M. S., & Nair, M. S. (2022). A computer-aided diagnosis system for the classification of COVID-19 and non-COVID-19 pneumonia on chest X-ray images by integrating CNN with sparse autoencoder and feed forward neural network. Computers in biology and medicine, 141, 105134.

[19] Banerjee, A., Sarkar, A., Roy, S., Singh, P. K., & Sarkar, R. (2022). COVID-19 chest X-ray detection through blending ensemble of CNN snapshots. Biomedical Signal Processing and Control, 78, 104000.

[20] Ismael, A. M., & Şengür, A. (2021). Deep learning approaches for COVID-19 detection based on chest X-ray images. Expert Systems with Applications, 164, 114054.

[21] Kanjanasurat, I., Tenghongsakul, K., Purahong, B., & Lasakul, A. (2023). CNN–RNN Network Integration for the Diagnosis of COVID-19 Using Chest X-ray and CT Images. Sensors, 23(3), 1356.

[22] Alshmrani, G. M. M., Ni, Q., Jiang, R., Pervaiz, H., & Elshennawy, N. M. (2023). A deep learning architecture for multi-class lung diseases classification using chest X-ray (CXR) images. Alexandria Engineering Journal, 64, 923-935.

[23] Kuzinkovas, D., & Clement, S. (2023). The detection of covid-19 in chest x-rays using ensemble cnn techniques. Information, 14(7), 370.

[24] Hafeez, U., Umer, M., Hameed, A., Mustafa, H., Sohaib, A., Nappi, M., & Madni, H. A. (2023). A CNN based coronavirus disease prediction system for chest X-rays. Journal of Ambient Intelligence and Humanized Computing, 14(10), 13179-13193.

[25] Shamrat, F. J. M., Azam, S., Karim, A., Ahmed, K., Bui, F. M., & De Boer, F. (2023). High-precision multiclass classification of lung disease through customized MobileNetV2 from chest X-ray images. Computers in Biology and Medicine, 155, 106646.

[26] Simonyan, K., & Zisserman, A. (2014). Very deep convolutional networks for large-scale image recognition. arXiv preprint arXiv:1409.1556.

[27] M. Sandler, A. Howard, M. Zhu, A. Zhmoginov and L. -C. Chen, "MobileNetV2: Inverted Residuals and Linear Bottlenecks," 2018 IEEE/CVF Conference on Computer Vision and Pattern Recognition, Salt Lake City, UT, USA, 2018, pp. 4510-4520, doi: 10.1109/CVPR.2018.00474.

[28] Krizhevsky, A. (2014). One weird trick for parallelizing convolutional neural networks. arXiv preprint arXiv:1404.5997.

[29] He, K., Zhang, X., Ren, S., & Sun, J. (2016). Deep residual learning for image recognition. In Proceedings of the IEEE conference on computer vision and pattern recognition (pp. 770-778).

[30] Szegedy, C., Vanhoucke, V., Ioffe, S., Shlens, J., & Wojna, Z. (2016). Rethinking the inception architecture for computer vision. In Proceedings of the IEEE conference on computer vision and pattern recognition (pp. 2818-2826).

[31] Huang, G., Liu, Z., Van Der Maaten, L., & Weinberger, K. Q. (2017). Densely connected convolutional networks. In Proceedings of the IEEE conference on computer vision and pattern recognition (pp. 4700-4708).

[32] Chollet, F. (2017). Xception: Deep learning with depthwise separable convolutions. In Proceedings of the IEEE conference on computer vision and pattern recognition (pp. 1251-1258).

[33] Akter, S., Shamrat, F. J. M., Chakraborty, S., Karim, A., & Azam, S. (2021). COVID-19 detection using deep learning algorithm on chest X-ray images. Biology, 10(11), 1174